S & M 4219

Ultrasensitive Detection of Dam Methyltransferase Based on DNA Tetrahedral Multi-toehold Dumbbells Coupled with Clustered Regularly Interspaced Short Palindromic Repeat/Cas12a System

Yuqi Huang,¹ Changlong He,¹ Shijia Ding,² Huacui Huang,³ Zhousong Xu,¹ Xiaoying Yang,¹ Dan Wu,¹ Zhongping Chen,^{1*} and Mingjun Zhang^{1**}

¹Clinical Laboratory, Chongqing Jiulongpo District People's Hospital, Chongqing 400050, China
²Key Laboratory of Clinical Laboratory Diagnostics (Ministry of Education), College of Laboratory Medicine, Chongqing Medical University, Chongqing 400016, China
³Clinical Laboratory, Chengdu Xindu District People's Hospital, Sichuan 610599, China

(Received September 1, 2025; accepted October 6, 2025)

Keywords: DNA methylation, Dam MTase, DNA tetrahedron, dumbbell ring, CRISPR/Cas12a, fluorescent biosensor

DNA methylation is critical for biological processes in prokaryotes and eukaryotes; its aberrations are tightly linked to the onset and progression of numerous diseases. As a key epigenetic component, it also sustains normal human cell function, regulates gene imprinting, and participates in oncogenesis. Clustered regularly interspaced short palindromic repeat (CRISPR)-based systems (e.g., CRISPR-Cas12a) are programmable and sensitive, making them valuable for biosensors—Cas12a exhibits unique trans-cleavage activity, randomly cleaving ambient single-stranded DNA (ssDNA) upon activation by target DNA. On the basis of this, we developed a sensitive assay for DNA methyltransferase (MTase) activity using the CRISPR-Cas system, employing a DNA tetrahedron with four dumbbell-ring-containing corners. In this assay, Dam MTase modifies the N6 position of adenine in the GATC sequence; the modified sequence is then cleaved by DpnI restriction endonuclease and associates with CRISPR-Cas12a. The exposed ssDNA activates Cas12a, which cleaves a fluorescent ssDNA probe to generate a signal—Dam MTase concentration is quantified via fluorescence intensity. This method detects Dam MTase in human serum, screens its inhibitor 5-fluorouracil (5-FU), and shows high sensitivity/specificity [linear range 0.01-1 U/mL ($R^2 = 0.99715$), limit of detection 0.001 U/mL]. It holds promise for early cancer diagnosis and clinical applications, representing a valuable research direction for related studies.

1. Introduction

DNA methylation is a widespread epigenetic modification, which is one of the earliest identified and most intensively studied epigenetic regulatory mechanisms. Broadly, DNA

^{*}Corresponding author: e-mail: 2572073760@qq.com

^{**}Corresponding author: e-mail: lijiankezhang@126.com https://doi.org/10.18494/SAM5876

methylation refers to the chemical modification process in which a specific base on a DNA sequence acquires a methyl group by covalent bonding under the catalytic action of DNA methyltransferase (DNMT) with S-adenosyl methionine (SAM) as the methyl donor. This DNA methylation modification can occur at sites such as the C-5 position of cytosine, the N-6 position of adenine, and the G-7 position of guanine. (1) DNA methylation is an important epigenomic epigenetic behavior of the genome in both eukaryotes and prokaryotes. (2) As a relatively stable state of modification, DNA methylation is inherited with the replication process of DNA by DNMTs to the nascent zygotic DNA and is an important epigenetic mechanism. Dam methyltransferase (MTase) is a methylation enzyme encoded by the chromosome of Escherichia coli and is a product of the Dam gene. The main principle is to methylate the N6 site of a specific adenine (A) in a DNA sequence. Specifically, Dam MTase recognizes the adenine in the sequence GATC and converts it to 6-methyladenine. For decades, 6mA-methyldeoxyadenine (N6-methyldeoxyadenine) has been considered to be widely present in prokaryotes, regulating DNA replication, repair, and transcription. (3) The abnormal DNA methylation status is associated with the disruption of DNMT activity, and abnormal enzyme activity is an important biochemical indicator of certain diseases. It can also lead to the development of genetic diseases and cancers. DNMTs are considered to be key biomarkers for the early clinical diagnosis. (4) Their main functions are reflected in monitoring pathogenic bacteria. Pathogenic bacteria that infect the human body, such as E. coli and Salmonella, rely on Dam MTase to regulate the expression of virulence genes. Detecting the activity of Dam MTase enables the assessment of bacterial virulence, thereby supporting the evaluation of infections as well as diagnosis and treatment. Assisting drug resistance analysis, the activity of Dam MTase in pathogenic bacteria affects the stability of drug resistance genes. The detection of Dam MTase activity can indirectly reflect the drug resistance ability of bacteria, providing a reference for the selection of antibiotics and supporting biotechnology. In scientific research, Dam MTase is used in experiments such as DNA modification and gene localization. It is necessary to detect its activity to ensure the reliability of the technology and the accuracy of the experiments. (5,6)

Dam MTase has emerged as a potential target for novel anticancer therapies and antimicrobial drugs. Therefore, it is crucial to develop a rapid, convenient, and sensitive method to monitor Dam MTase activity. The ultrasensitive detection of Dam MTase is important for biomedical research and clinical diagnosis owing to its profound impact on gene regulation.

The traditional methods for the detection of Dam MTase include high-performance liquid chromatography,⁽⁷⁾ radioactivity analysis,⁽⁸⁾ electrophoresis,⁽⁹⁾ and reverse transcription polymerase chain reaction (RT-PCR).⁽¹⁰⁾ However, these methods have the disadvantages of cumbersome experimental operation, high detection cost, and being time-consuming. Therefore, the design of a fast, simple, and ultrasensitive detection method came into being. DNA tetrahedral nanostructures (DTNs) have good programmability and tissue permeability. DTNs are nanomaterials with high mechanical stiffness, stability, and tetragonal toeholds with functional modification sites. Therefore, DTNs have shown promising applications in biodetection, imaging, and drug delivery, and as gene carriers. It has been reported that DTNs as gene carriers can be used as loading carriers for nucleic acid molecules, which have proved to be valuable in delivering various bioactive molecules.^(11,12) Because of the base complementary

pairing rule, DTNs present a typical three-dimensional structure. Compared with twodimensional single-stranded DNA (ssDNA) and double-stranded DNA (dsDNA), a DTN carries signaling material, which is an important mediator for efficient fluorescence generation and provides an important carrier function for the reaction of Cas12a enzyme. (13) Whereas a clustered regularly interspaced short palindromic repeat (CRISPR) is a promising technology in biology, as one of the CRISPR-associated (Cas) proteins of Cas12a, an RNA-guided nuclease in the V-type CRISPR-Cas system, it is a powerful gene-editing tool. In 1987, Japanese researchers discovered an alkaline phosphatase gene in E. coli, K19, near the alkaline phosphatase gene near a tandem repeat spacer sequence, which was later found to be widespread in bacteria. The sequence was named "clustered regularly interspaced short palindromic repeat sequence" (CRISPR) in 2002. (14) The CRISPR-Cas12a system forms a DNA cleavage-capable complex with crRNA and exerts its trans-cleavage activity by recognizing the PAM site on the target pathogen gene. After amplifying the pathogenic gene, visualization materials such as fluorescent probes are added to the detection system, while the CRISPR system has the advantages of rapid detection and high sensitivity, allowing a faster and more accurate diagnosis of pathogenic bacteria. (15) The mechanism of the CRISPR-Cas system programmed by CRISPR-guided RNA or crRNA cuts both the target nucleic acid and all neighboring nucleic acids indiscriminately. This target-triggered incidentally active CRISPR-Cas system has stimulated the development of CRISPR-based biosensing technology, as it has the unique advantages of simple fabrication, ultrahigh sensitivity, high specificity for single-base variants, and good diagnostic capability for POC. (16) The scheme of a fluorescent biosensor based on a DNA tetrahedron combined with a CRISPR/Cas system for the detection of DNA methylation transferase is reported for the first time. Other methods such as electrochemical biosensors, (17-20) colorimetric methods, (21,22) and chemiluminescence^(23,24) have the disadvantages of unstable detection and high false-positive rate, but the proposed scheme can greatly improve the detection efficiency. In this scheme, we design the DNA tetrahedron with the dumbbell strand in each toehold, where the 5' end of each tetrahedron is modified with P and the 3' end is still OH. The two ends are combined under the catalytic action of T4 DNA ligase, and the structure of the tetrahedron and the dumbbell are both very stable under certain reaction conditions. The dumbbell has the recognition site 5'-GATC-3' of Dam MTase. After the formation of this structure, a different concentration of Dam MTase recognizes and methylates the site. This is followed by the recognition of Dpn I restriction endonuclease, exposing the CRISPR/Cas12a system crRNA binding part, after the formation of the whole reaction system, and also in the presence of FQ-ssDNA, which emits fluorescence under the shear action of CRISPR/Casl2a and produces corresponding fluorescence signals according to the different concentration of Dam MTase, while in the absence of Dam MTase, almost no fluorescence is produced, the matrix effect of the reaction is also very weak, and the scheme also verifies the 5-fluorouracil (5-FU) inhibition of Dam MTase, and finally, the reaction enables the detection of the enzyme in human serum. The implementation of this scheme not only improves clinical drug therapy and provides an important reference value, but also greatly assists the clinical aspects of early detection, diagnosis, and early treatment.

2. Materials and Methods

2.1 Materials and reagents

All DNA oligonucleotides and crRNAs used in this study were synthesized by Sangon Biotech. Co., Ltd. (Shanghai, China) and purified by HPLC. The detailed sequences of these oligonucleotides are shown in Table 1. EnGen Lba Cas12a (Cpf1), Dam MTase, T4 DNA ligase, Dpn I methylation restriction endonuclease, M.Sss I MTase, and the corresponding buffers were purchased from NEB Co., Ltd. (Beijing, China). 5-FU was purchased from Solarbio Bio. (Beijing, China). TE buffer, tris(hydroxy methyl)aminomethane (Tris) powder, magnesium chloride hexahydrate (MgCl₂–6H₂O) reagent, ammonium persulfate (APS), acrylamide/methylenebisacrylamide 30% solution (29:1), N,N,N',N'-tetramethylethylenediamine (TEMED), and 5×TBE buffer were purchased from Sangon Biotech. Co., Ltd. (Shanghai, China). The third-generation Gelred nucleic acid staining solution was purchased from Mei5 Biotechnology Co., Ltd. (Beijing, China). The RNase inhibitor, 20 bp DNA ladder, 1000 bp DNA marker, and 6×loading buffer were purchased from Takara Biotech Co., Ltd. (Beijing, China). All DNA oligonucleotides were dissolved in TE buffer, crRNA was dissolved in DEPC water, and both were stored at -20 °C for subsequent experiments. All reagents were of analytical grade and were not further purified. RNase-free water was used throughout the experiments.

Table 1 Oligonucleotide sequences used in this work

Name	Sequence (5'→3')			
Dumbbell chain	P- TCAGCTTAGTACATTGCTGATCAGCTTAGTACATTGCTGA			
	P-TCAACTGCCTGGTGATAAAACGACACTACGTGGGAATCT			
S1	ACTATGGCGGCTCTTCTCAGCTTAGTACATTGCTGATCAGC			
	TTAGTACATTGCTGA			
	P-ACATTCCTAAGTCTGAAACATTACAGCTTGCTACACGAGA			
S2	AGAGCCGCCATAGTATCAGCTTAGTACATTGCTGATCAGCTT			
	AGTACATTGCTGA			
S3	P-TATCACCAGGCAGTTGACAGTGTAGCAAGCTGTAATAGATG			
	CGAGGGTCCAATACTCAGCTTAGTACATTGCTGATCAGCTTA			
	GTACATTGCTGA			
	P-TTCAGACTTAGGAATGTGCTTCCCACGTAGTGTCGTCTGTAT			
S4	TGGACCCTCGCATTCAGCTTAGTACATTGCTGATCAGCTTAGT			
	ACATTGCTGA			
S1'	P-TCAACTGCCTGGTGATAAAACGACACTACGTGGGAATCTAC			
	TATGGCGGCTCTTC			
S2'	P-ACATTCCTAAGTCTGAAACATTACAGCTTGCTACACGAGAA			
	GAGCCGCCATAGTA			
S3'	P-TATCACCAGGCAGTTGACAGTGTAGCAAGCTGTAATAGATG			
	CGAGGGTCCAATAC			
S4'	P-TTCAGACTTAGGAATGTGCTTCCCACGTAGTGTCGTCTGTAT			
	TGGACCCTCGCAT			
crRNA	UAAUUUCUACUAAGUGUAGAUUCA GCA AUG UAC UAA GCU GA			
F-Q reporter	FAM-TTATT-BHQ1			

2.2 Equipment

Atomic force microscopy (AFM) imaging was performed using a Dimension Icon instrument (Bruker Nano GmbH, Berlin, Germany). All fluorescence spectral results were obtained from an F-4700 fluorescence spectrophotometer (Hitachi, Japan) using a quartz fluorescence cuvette with an optical range length of 1.0 cm. Detection parameters were set to an excitation wavelength of 490 nm, an emission wavelength of 500–600 nm, and excitation and emission slits of 5 nm. The synthesis of DNA tetrahedron and dumbbell, and DNA methylation cleavage reactions were accomplished in a B1000 thermocycler (Bio-Rad, USA). Non-denaturing polyacrylamide gel electrophoresis (native PAGE) was carried out on an electrophoresis analyzer (Liuyi Bio., Beijing, China), and the results were displayed on an imager (Servicebio, Wuhan, China). The dry powder of this oligonucleotide was pre-centrifuged at a high speed at 4 °C (Thermo Fisher, USA). AFM imaging was performed using a Dimension Icon instrument (Bruker Nano GmbH, Berlin, Germany).

2.3 Synthesis of DNA tetrahedron

The successful synthesis of the dumbbell-shaped DTN (bDTN) was verified by 8% native PAGE and AFM. The synthesis process was as follows. First, four strands of DNA tetrahedron (dry powder) were centrifuged in a precooled 4 °C high-speed centrifuge at 12000 g for 10 min and then placed on ice. A certain amount of TE buffer was accurately added and the mixture was swirled three times for complete dissolution to 100 μ M. Then, the solution was heated at 95 °C for 5 min in the B1000 thermocycler and the temperature was rapidly lowered to 4 °C for 30 min to induce the reaction to form DTN. The bDTN formation conditions are heating at 95 °C for 5 min, 37 °C for 30 min, and finally 4 °C for 30 min. The 2 μ M reaction products were stored at –20 °C in a refrigerator. DNA tetrahedron was synthesized in TM buffer (20 mM Tris and 50 mM MgCl₂-6H₂O).

Each single strand of S123, S124, S134, S234, and S1234 (at a concentration of 0.5 μ M) was mixed with 2 μ L of 6×loading buffer, added to the electrophoresis gel, and run for 35 min in the electrophoresis instrument with power set to 100 V. The gel was removed and stained for 50 min in 50 mL of 1×TBE buffer containing 2 μ L of nucleic acid stain and finally imaged in a gel imager.

2.4 DNA methylation reaction

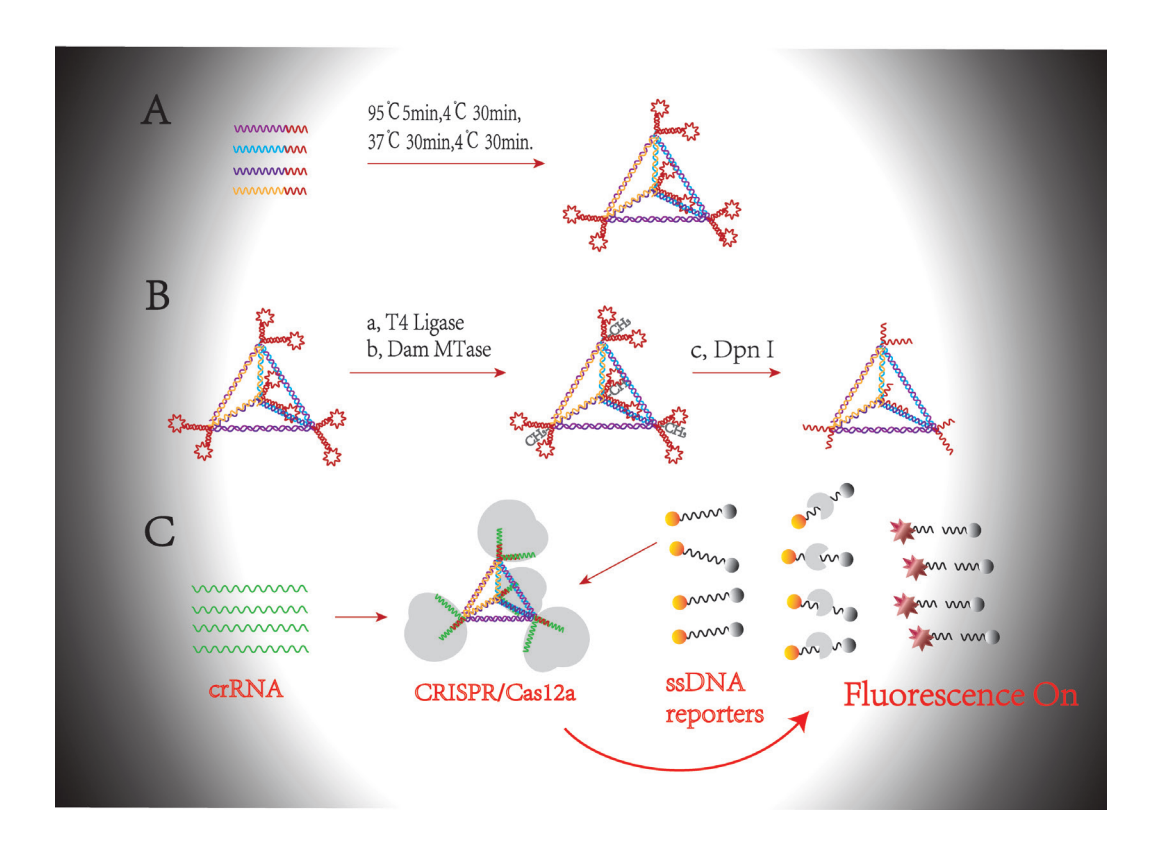
The entire DNA methylation reaction was initiated with the synthesis of bDTN. $^{(25,26)}$ Feasibility verification was performed as follows: first, the concentration of bDTN was adjusted to 2 μ M. ssDNA (S1–S4) dry powder was dissolved to a final concentration of 100 μ M. For the assembly of bDTN, 1 μ L of each solution from S1 to S4 and 46 μ L of TM buffer were mixed, transferred to a B1000 thermocycler, and incubated at 95 °C for 5 min. The mixture was then cooled to 4 °C for 30 min, followed by incubation at 37 °C for 30 min to promote dumbbell formation, and finally held at 4 °C for 30 min. The resulting bDTNs were stored at 4 °C for

subsequent use. To stabilize the dumbbell structure, a T4 DNA ligase-mediated ligation reaction was performed. The 5'-ends of the DNA tetrahedron single strands were pre-modified with phosphate groups (P), enabling ligation between the 5'-phosphate and 3'-hydroxyl ends upon the addition of T4 DNA ligase. In this step, the bDTN concentration was adjusted to 1 µM. The reaction mixture was supplemented with 400 U of T4 DNA ligase and its buffer, incubated at 16 °C for 1 h, and then heated at 70 °C for 10 min to inactivate the enzyme, ensuring complete ligation. The subsequent critical step was the DNA methylation reaction conducted at a bDTN concentration of 0.75 μM. The methylation mixture contained 100 U/mL Dam MTase, 160 μM S-adenosylmethionine (SAM), and 5 μL of 10×Dam MTase reaction buffer, with a total reaction volume of 50 μL. This reaction was incubated at 37 °C for 45 min in a thermocycler. For the subsequent Dpn I digestion, the bDTN concentration was adjusted to 0.5 μM. To the reaction system, 9 U of Dpn I restriction endonuclease and 5 μL of 10×rCutSmartTM buffer were added, and the 50 μL mixture was incubated at 37 °C for 40 min. The final fluorescence reaction was performed at a bDTN concentration of 0.4 µM in a 50 µL reaction mixture, which contained 0.25 μM Casl2a, 0.25 μM crRNA (pre-supplemented with the RNase inhibitor), and 0.1 μM fluorescent ssDNA. The reaction was incubated at 37 °C for 35 min, protected from light, and then analyzed using a Hitachi F-4700 fluorescence detector. Prior to detection, enzyme-free water was added to adjust the total volume to 100 μL, resulting in a final bDTN concentration of $0.2 \mu M.$

3. Results and Discussion

3.1 Dam MTase detection strategy

Scheme 1 shows an outline of the detection mechanism for Dam MTase based on bDTN integrated with the CRISPR/Cas12a system. As shown in Part A, bDTN is assembled stably under optimized conditions. The dumbbell motifs at each vertex of the bDTN tetrahedron are derived from 40-base single strands that fold into dumbbell conformations under specific conditions, serving as structurally identical toeholds. Each of the four constituent strands (S1– S4) of bDTN contains two functional domains, namely, a 55-base tetrahedral segment, where each 17-base segment undergoes complementary base pairing with corresponding regions of other strands, and a 40-base dumbbell segment composed of two identical 20-base subunits. Notably, the 5' ends of S1-S4 are phosphorylated, while the 3' ends retain hydroxyl groups; these termini are ligated by T4 DNA ligase to form covalently closed loops. (27) Following dumbbell formation, sequential DNA methylation and enzymatic cleavage reactions are performed. The dumbbell structure, stabilized by constrained base pairing, gives rise to two identical singlestranded segments that enable the subsequent CRISPR/Cas12a-mediated cleavage reaction. The cleavage of the fluorescently labeled ssDNA reporter yields a fluorescence signal whose intensity is positively correlated with Dam MTase concentration. The efficient synthesis of bDTN was validated as shown in Fig. 1. In Part B, after the stable assembly of bDTN, T4 DNA ligase is introduced to ligate the 5'-phosphorylated termini to the 3'-hydroxyl termini of each strand, enhancing structural stability. The subsequent DNA methylation reaction involves Dam



Scheme 1. (Color online) Schematic illustration of ultrasensitive Dam MTase detection employing DNA tetrahedral multi-toehold dumbbells coupled with CRISPR/Cas12a system. (A) Assembly process of the bDTN nanostructure. (B) Progression of the DNA methylation reaction. (C) Interaction between bDTN and CRISPR/Cas12a triggering fluorescence generation.

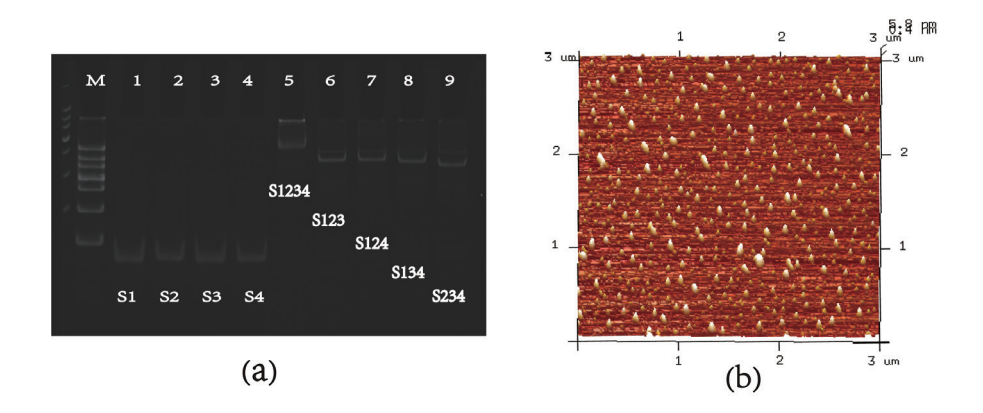
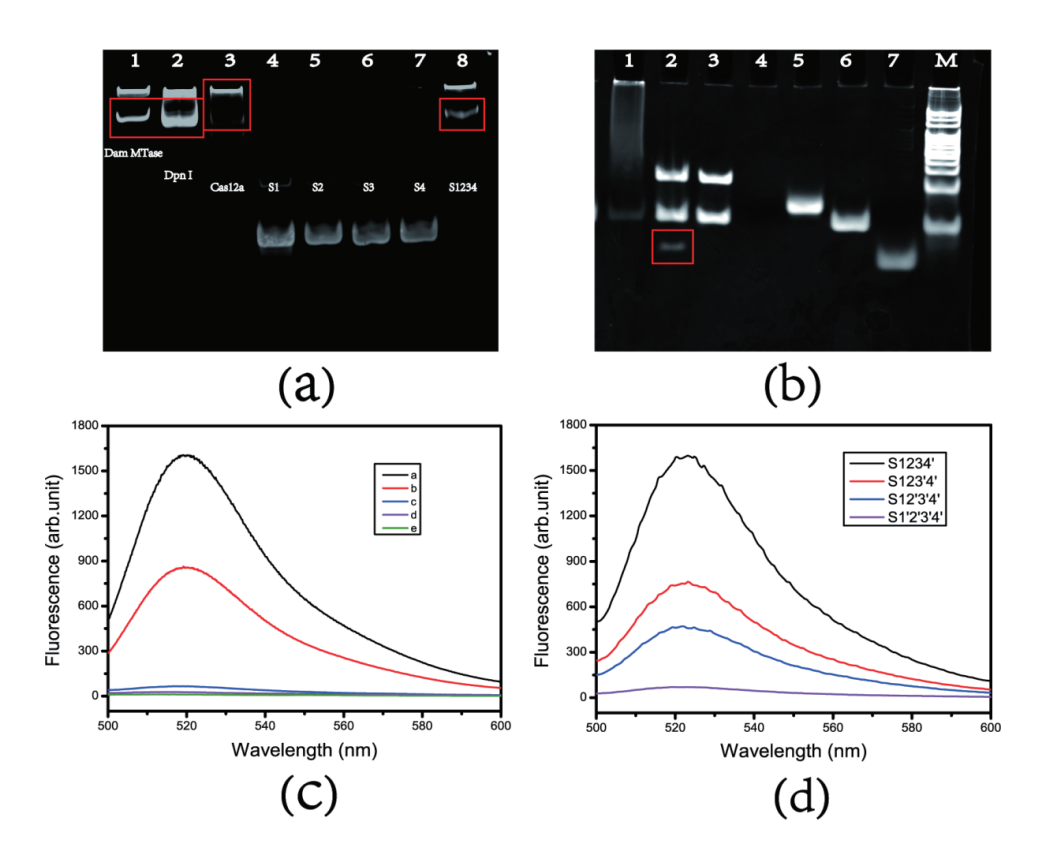


Fig. 1. (Color online) Characterization of the DTN. (a) 8% native PAGE of the bDTNs. From left to right: lane M, 1000 bp DNA marker; lanes 1 to 4, single-stranded S1, S2, S3, and S4; lanes 6 to 9, S123, S124, S134, and S234 (the above three figures depict the three-dimensional structures formed by three strands); lane 5, S1234 (bDTNs). (b) AFM image of the bDTNs.

MTase recognizing the 5'-GATC-3' motif and transferring methyl groups from SAM to adenine residues, thereby generating Dpn I cleavage sites within the tetrahedral dumbbell loops. 5'-GATC-3' is the recognition site for Dpn I and is cleaved by Dpn I only when A (adenine) is

methylated. Cleavage by Dpn I exposes single-stranded segments that interact with the CRISPR/Cas12a system, facilitating the reaction cascade depicted in Part C. In Part C, CRISPR/Cas12a forms a complex with crRNA and exhibits trans-cleavage activity towards the fluorescently labeled ssDNA reporter. This reporter is modified with a FAM fluorophore at the 5' end and a BHQ1 quencher at the 3' end; cleavage separates these moieties, resulting in the release of a measurable fluorescence signal. This protocol achieves a high signal-to-noise ratio for fluorescence detection, providing a robust basis for subsequent validation assays, including Dam MTase detection in human serum and 5-FU inhibition studies.

To verify the feasibility of the reaction, we first synthesized bDTN in TM buffer. The successful synthesis of bDTN was validated via 8% native PAGE, as shown in Fig. 1(a). From left to right, the lanes contain 1000 bp DNA marker; lanes 1-4, the four individual strands (S1-S4) of bDTN; lane 5, intact bDTN; lanes 6–9, bDTN formed by three strands (S123, S124, S134, and S234). The results demonstrate the efficient synthesis of bDTN, confirming the feasibility of subsequent experiments. All assayed samples were prepared at a concentration of 0.2 μM. Additionally, the structure of bDTN was validated by AFM, as presented in Fig. 1(b) (synthesized by the aforementioned method and diluted to 1 µM for imaging). In the AFM micrograph, typical DNA tetrahedrons are visualized as discrete granular or quasi-spherical dots. The dispersibility of DNA tetrahedrons directly affects their biological applications, including cellular delivery and biosensing, with AFM imaging providing a straightforward means to assess their dispersion behavior. Observations demonstrating uniform morphology and good dispersibility confirm that bDTN has undergone efficient self-assembly, thereby meeting the structural criteria for subsequent applications in nanomedicine and biosensing. Next, we validated the whole reaction process with 8% native Page, as shown in Fig. 2(a). From left to right, lane 1 shows that, subsequent to the assembly of bDTN, the DNA methylation reaction is executed. After S1-S4 formed a dumbbell-shaped DNA tetrahedron and the methylated site was formed, Dam MTase was added. Dam recognized the methylated site to achieve the DNA methylation reaction. This indicates that the band showed no significant change in the methylation reaction with Dam MTase added compared with the simple S1234 tetrahedron, while the band concentration increased when the enzyme was added to modify methyl groups during the methylation reaction, which was consistent with the reaction phenomenon. Lane 2 corresponds to the sample where bDTN, after undergoing DNA methylation, was further subjected to enzymatic cleavage with the specific endonuclease Dpn I. This cleavage reaction did not alter the size of the bDTN band; however, the band intensity increased progressively with the elevation of enzyme concentration. Lane 8 displays the directly synthesized bDTN without subsequent reactions, thus exhibiting electrophoretic migration identical to those of lanes 1 and 2. Notably, the band corresponding to the simply synthesized bDTN appeared relatively faint in intensity. As can be seen from the bands, the addition of crRNA triggered the reaction of Casl2a, resulting in the cleavage of the nucleic acid strand in the toehold region of bDTN. Consequently, the concentration of bDTN decreased, the total number of bases in the structure decreased, and the color of the band became lighter, which was consistent with the reaction. Lanes 4-7 correspond to the four long strands of bDTN, with the concentrations of S1-S4 being maintained at 1 µM in these lanes. In contrast, the product concentrations in the remaining lanes were



(Color online) Validation of feasibility. (a) 8% native PAGE of complete fluorescence reaction (from the formation of bDTNs to the enzymatic cleavage reaction of Cas12a bound to bDTNs). From left to right: lane 1, subsequent to the assembly of bDTNs, the DNA methylation reaction is executed; lane 2, subsequent to the DNA methylation reaction of bDTNs, Dpn I restriction endonuclease was introduced to execute methylated-site-specific enzymatic cleavage; lane 3, following Dpn I-mediated cleavage, Cas12a, crRNA, and fluorescent ssDNA were cointroduced to trigger the enzyme-catalyzed fluorescent cleavage reaction; lanes 4 to 7, single-stranded S1, S2, S3, and S4; lane 8, bDTNs. (b) 8% native PAGE analysis of fluorescence responses generated by the binding of various DNA strands to the CRISPR/Cas12a system. From right to left: lane 7, semi-DRs incubated with the CRISPR/Cas12a system; lane 6, dumbbell chains incubated with the CRISPR/Cas12a system; lane 5, crRNA incubated with the CRISPR/Cas12a system; lane 4, fluorescent ssDNA incubated with the CRISPR/Cas12a system (which, owing to its small length, was not clearly visualized); lane 3, methylated DRs; lane 2, semi-DRs generated via Dpn I-mediated cleavage of DRs; lane 1, the fluorescent enzymatic cleavage reaction integrating the CRISPR/Cas12a system subsequent to methylation and Dpn I-cleavage reaction. (c) The feasibility of the protocol is validated by the magnitude of fluorescence intensity. The curves are defined as follows: curve a, the fluorescence-based enzymatic cleavage reaction integrating the CRISPR-Cas12a system with bDTN methylation and Dpn I-mediated cleavage; curve b, the fluorescence-based enzymatic cleavage reaction integrating the CRISPR-Cas12a system with the methylation of DRs and Dpn I-mediated cleavage; curve c, the fluorescence-based enzymatic cleavage reaction integrating the CRISPR-Casl2a system with the methylation of semi-DRs and Dpn I-mediated cleavage; curve d, the fluorescence reaction involving single-stranded dumbbells bound to the CRISPR-Cas12a system for Dam MTase detection; curve e, fluorescent ssDNA alone. (d) The curves validate the fluorescence intensity of the CRISPR/ Cas12a-based fluorescent enzymatic cleavage reaction, which follows the methylation of bDTN and DTN (formed by the four strands S1-S4 and S1'-S4') and is dependent on the number of strands containing DRs. From top to bottom, (a) shows the fluorescence intensity of the S1234' tetrahedron following methylation and subsequent integration with the CRISPR/Cas12a-based fluorescent enzymatic cleavage reaction; (b) the fluorescence intensity of the S123'4' tetrahedron following methylation and subsequent integration with the CRISPR/Cas12a-based fluorescent enzymatic cleavage reaction; (c) the fluorescence intensity of the S12'3'4' tetrahedron following methylation and subsequent integration with the CRISPR/Cas12a-based fluorescent enzymatic cleavage reaction; (d) the fluorescence intensity of the S1'2'3'4' tetrahedron following methylation and subsequent integration with the CRISPR/Cas12a-based fluorescent enzymatic cleavage reaction (notably, no fluorescent reaction occurs when all long strands are devoid of DRs).

prepared as follows. Initially, the concentration of bDTN was 2 μM; subsequent to the addition of T4 DNA ligase, the concentration of bDTN was adjusted to 1 µM; after methylation modification, the concentration of bDTN was 0.75 µM; following the digestion reaction induced by the addition of the Dpn I enzyme, the concentration of bDTN decreased to 0.5 μM; and finally, upon the addition of Cas12a for fluorescence detection, the concentration of bDTN was 0.4 µM. In Fig. 2(b), we can simply verify the fluorescence responses generated by the binding of various DNA strands to the CRISPR/Cas12a system. From right to left, lane 7 is for the semidumbbell ring (the dumbbell chain is a 40-base symmetric chain that forms a cyclic structure upon the addition of T4 DNA ligase, while the semi-dumbbell chain is a DNA chain containing 20 bases), lane 6 is for the dumbbell ring (DR), lane 5 is for crRNA, and lane 4 is for fluorescent ssDNA (owing to the small number of bases in the strand, the band was not clearly visible). The 40-base DR is a dumbbell-shaped cyclic structure formed by the dumbbell chain upon the addition of T4 DNA ligase. Simultaneously, the DNA methylation reaction occurs during the formation of the Dam MTase recognition site. Lane 3 corresponds to the DNA methylation reaction of the DRs, and it can be visually observed that this band migrates more slowly than that of the dumbbell chain. Lane 2 corresponds to the product obtained by subjecting the methylated DR (from lane 3) to the Dpn I specific endonuclease reaction. The methylated sites were recognized, and Dpn I identified the corresponding sites and cleaved the dumbbell neck, resulting in the formation of two identical semi-DRs. These semi-DRs were unstable and thereby dissociated into 20-base single strands. Finally, lane 1 corresponds to the product of the fluorescence reaction, which was generated as follows. After the formation of bDTNs, the toeholds of bDTNs underwent the DNA methylation and Dpn I digestion reactions, and were ultimately combined with Cas12a and crRNA, followed by the addition of fluorescent ssDNA to initiate the CRISPR/Cas12a-based enzyme cleavage reaction. It could be observed that the band exhibited the lowest migration rate, which was consistent with the reaction phenomenon. The concentration of all products in these lanes was 2 µM. In Fig. 2(c), we validated the feasibility of our proposed protocol by quantifying the magnitude of fluorescence intensity. Specifically, curve a corresponds to the complete fluorescence reaction system, encompassing the formation of bDTNs followed by DNA methylation and culminating in the Cas12a-mediated enzymatic cleavage reaction, which displayed the strongest fluorescence signal. Curve b represents the fluorescence signal generated subsequently to the DNA methylation and Dpn I treatment of the DRs. Curve c corresponds to the fluorescence-based enzymatic cleavage reaction incorporating the CRISPR-Casl2a system, which integrates the methylation of semi-DRs and Dpn I-mediated cleavage. Curve d denotes the fluorescence signal from the single-stranded dumbbell binding to the CRISPR-Cas12a system, as employed for detecting Dam MTase. Curve e corresponds to fluorescent ssDNA alone. Collectively, these findings demonstrate that the CRISPR-Cas12a system exhibits robust enzymatic activity toward diverse single-stranded substrates, thereby triggering fluorescence signal generation from fluorescent ssDNA upon catalytic cleavage. This further substantiates both the CRISPR-Cas12a-mediated enzymatic cleavage mechanism we postulated in our strategy and the viability of the overall approach. Using Fig. 2(d), we evaluated the fluorescence intensity profiles of DNA tetrahedrons with different numbers of long strands (S1234', S123'4', S12'3'4', and S1'2'3'4') during the following process: bDTNs undergoing DNA

methylation, followed by their integration with the CRISPR/Cas12a-based fluorescent enzymatic cleavage reaction. From top to bottom, the curves correspond sequentially to experimental groups containing only the short strand S4' (in the absence of dumbbell strands) while the other three strands are all long strands, namely, S1, S2, and S3, which contain 40-base DRs; the short strands S3' and S4' (without dumbbell strands) with the other two strands being long strands, namely, S1 and S2, which contain 40-base DRs; the short strands S2', S3', and S4' (without dumbbell strands) with only S1 as the long strand, which contains a 40-base DR; and the short strands S1', S2', S3', and S4' (all strands without dumbbells), where S1'-S4' can only form a DNA tetrahedron without DRs. Notably, the fluorescence signal remained relatively robust even when only one long chain was excluded from the reaction system. The experimental procedure for verifying the feasibility of the reaction was as follows. First, DNA bDTN was synthesized at a concentration of 2 µM. In the second step, T4 DNA ligase and its buffer were added, which diluted the bDTN concentration to 1 μM. The third step involved the DNA methylation reaction, where Dam MTase, SAM, and the corresponding buffer were introduced, diluting the bDTN concentration to 0.75 µM. Following the methylation reaction, specific endonuclease digestion with Dpn I was performed, and the bDTN concentration was further adjusted to 0.5 μM. In the final step, the Cas12a cleavage reaction was conducted by co-adding Cas12a, crRNA, and fluorescent ssDNA, resulting in a bDTN concentration of 0.4 μM. For each of the above steps, enzyme-free water was added to adjust the reaction volume to 50 μL. For fluorescence detection, an additional 50 μ L of enzyme-free water was added to bring the total volume to 100 μ L, thereby diluting the bDTN concentration to 0.2 μM.

3.2 Optimization of experimental conditions

To achieve maximal efficiency in detecting Dam MTase, we optimized several experimental conditions. We quantified the direct fluorescence signals as follows. For each experimental segment, we validated blank signals in the absence of the target, and the trend of the signal-tonoise ratio (F/F_0) was found to be approximately equivalent to F. First, we optimized the concentration of bDTN, as an appropriate bDTN concentration is critical for the subsequent experiments. As depicted in Fig. 3(a), the fluorescence signal increased progressively with increasing bDTN concentration, reaching a maximum at 2 µM. With further increase in bDTN concentration, the fluorescence signal decreased. Thus, 2 µM was selected as the optimal bDTN concentration for subsequent reactions. Next, we evaluated the effect of the Dpn I concentration on the cleavage of bDTN dumbbells. The cleavage efficiency increased with the Dpn I concentration, accompanied by a gradual increase in fluorescence signal. However, excessive Dpn I inhibited the reaction: as shown in Fig. 3(b), the fluorescence signal peaked at 12 U Dpn I, whereas further increase in Dpn I concentration led to a decrease in fluorescence. Therefore, 12 U was determined to be the optimal Dpn I concentration. We also optimized the reaction times for Dam MTase (methylation step) and Dpn I (cleavage step), as these parameters affect experimental efficiency. Enzyme consumption increased with prolonged reaction, affecting reaction stability. For Dam MTase [Fig. 3(c)], the fluorescence intensity increased with reaction time, reaching a maximum at 45 min; further extension of the reaction time resulted in a slight

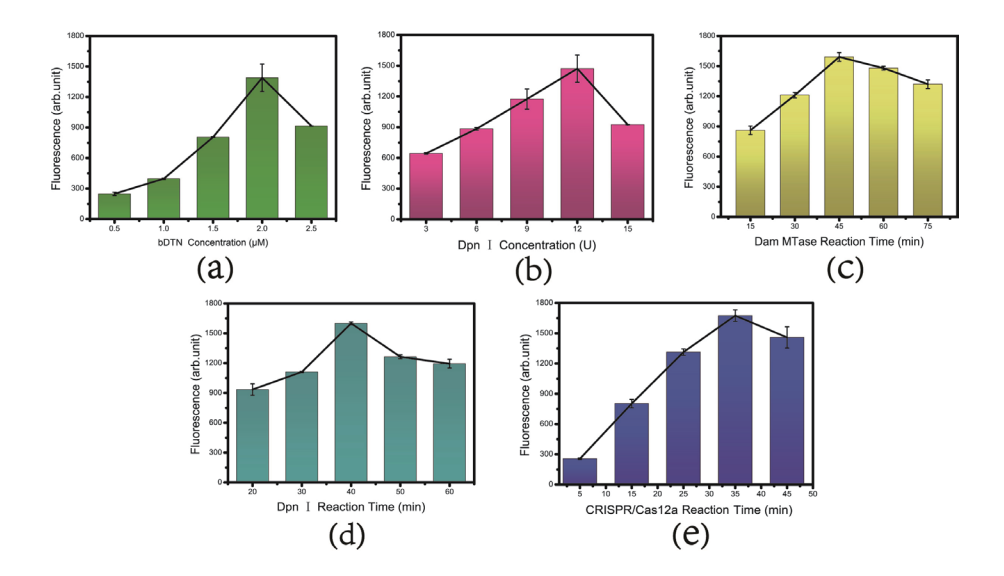


Fig. 3. (Color online) Optimization of experimental conditions. (a) Optimization of bDTN concentration. (b) Optimization of Dpn I concentration. (c) Optimization of Dam methylation reaction duration. (d) Optimization of Dpn I reaction duration. (e) Optimization of CRISPR/Cas12a reaction duration. [Error bars indicate standard deviations (SDs); all experiments were independently performed three times (n = 3), with three technical replicates per experiment.]

decrease in signal. Thus, 45 min was chosen as the optimal methylation time. For Dpn I [Fig. 3(d)], the fluorescence intensity peaked at 40 min, with a subsequent decrease upon prolonged incubation, so 40 min was selected as the optimal cleavage time. Finally, the fluorescence reaction time of the CRISPR/Cas12a system is critical for detection. Following the stable addition of crRNA and fluorescent ssDNA, the fluorescence signal changed dynamically with the enzymatic cleavage reaction: it increased gradually but decreased upon prolonged incubation at 37 °C. Therefore, reaction products should be promptly stored at 0–4 °C in the dark. As shown in Fig. 3(e), the optimal reaction time was 35 min, with timely detection recommended.

3.3 Linear assay

Under optimal conditions, we conducted a linear detection assay for Dam MTase, with Dam MTase concentrations ranging from 0 to 50 U/mL. As depicted in Fig. 4(a), fluorescence measurements were performed for the following serially diluted Dam MTase concentrations: 0, 0.001, 0.002, 0.004, 0.006, 0.008, 0.01, 0.02, 0.06, 0.1, 0.5, 1, 10, and 50 U/mL. Notably, the fluorescence intensity increased with the target concentration. Figure 4(b) illustrates a positive curvilinear relationship between the fluorescence intensity and the target concentration, while Fig. 4(c) reveals a positive linear correlation within the concentration range of 0.01–1 U/mL. The linear calibration equation was determined as y = 831.67 + 280.77x with a high correlation coefficient ($R^2 = 0.99715$), indicating excellent linearity. The limit of detection (LOD) was calculated using the $3\sigma/S$ criterion (where σ is the SD of blank signals and S is the slope of the linear calibration curve) to be 0.001 U/mL. A comparison with previously reported Dam MTase

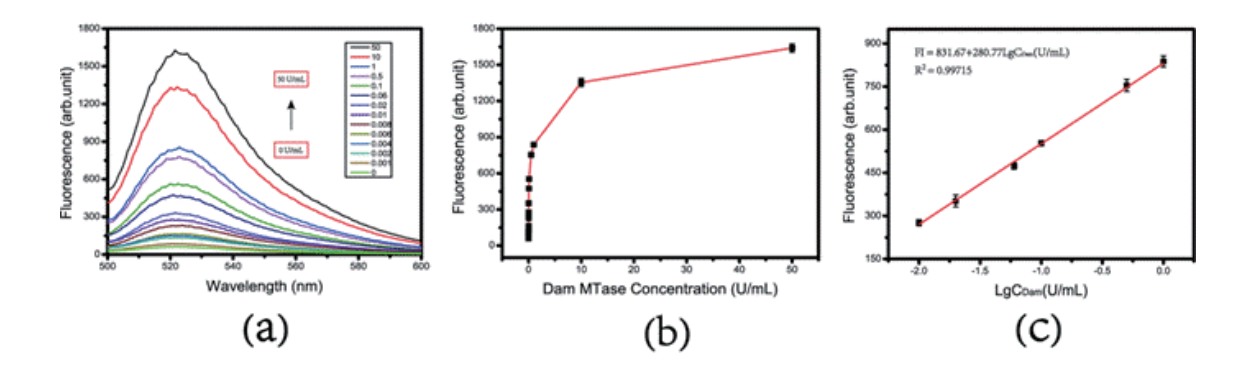


Fig. 4. (Color online) Linearity validation. (a) Fluorescence intensity profiles across a gradient of Dam MTase concentrations: 0, 0.001, 0.002, 0.004, 0.006, 0.008, 0.01, 0.02, 0.06, 0.1, 0.5, 1, 10, and 50 U/mL. (b) Scatter plot of fluorescence signals plotted against corresponding Dam MTase concentrations. (c) Linear calibration curve of fluorescence intensity over the concentration range of 0.01–1 U/mL. [Error bars indicate SDs; all experiments were independently performed three times (n = 3), with three technical replicates per experiment.]

detection methods (Table 2) indicated that our assay exhibits excellent stability and high sensitivity.

3.4 Specificity and stability verification

To validate the specificity of the Dam MTase assay, fluorescence signals were measured for M.SssI MTase alone and for the co-incubation system of Dam MTase with M.SssI MTase under the same experimental conditions as described in Fig. 5. Dam MTase specifically recognizes the 5'-GACT-3' sequence, whereas CpG MTase M.SssI catalyzes the methylation of the C5 position of all cytosine residues within the double-stranded 5'-CG-3' recognition motif. Notably, with the coexistence of Dam MTase and M.SssI MTase, the inhibition of Dam-mediated reactions occurs even in the absence of M.SssI-specific recognition sites. This inhibition is attributed to non-substrate-dependent mechanisms, including competition for SAM, protein–protein interactions, nonspecific DNA binding, and microenvironmental perturbations. These findings indicate that enzymatic crosstalk is not solely reliant on specific substrates; instead, indirect modalities such as resource competition and physical interference can modulate mutual functionality, thereby resulting in diminished fluorescence intensity. All enzymes were used at a concentration of 50 U/mL. These results confirm that the successful execution of the subsequent fluorescence assay is contingent upon the specific recognition of the corresponding site on the bDTN dumbbell structure by Dam MTase.

As illustrated in Fig. 6, we further validated the stability of the fluorescence reaction. The CRISPR/Cas12a system exhibits a time-dependent limitation in reaction stability: over the course of the assay, a gradual decrease in fluorescence intensity was observed from day 2 to day 10. On a daily timescale, the diminution of fluorescence in the CRISPR/Cas12a system arises from the synergistic effects of fluorophore chemical degradation, the hydrolysis of labeled

Table 2 Highly sensitive fluorescence strategies for the detection of Dam MTase.

Detection method	Detection strategy	Detection concentration range	Linear analysis range	LOD
Fluorescence ⁽²⁸⁾	SDA coupled with RCA	0 to 4 U/mL	0.02 to 4 U/mL	0.0067 U/mL
Fluorescence ⁽²⁹⁾	poly-T Cu NCs engineered by TdTase	1 to 300 U/mL	1 to 300 U/mL	0.176 U/mL
Fluorescence ⁽³⁰⁾	Multiple sealed primers-mediated RCA strategy	0.05 to 320 U/mL	0.05 to 10 U/mL	0.0085 U/mL
Fluorescence ^{[(31)}	AuNSTs@SiO2@ Cy5.5-based PEF probe	0.1 to 16 U/mL	0.1 to 16 U/mL	0.037 U/mL
Fluorescence ⁽³²⁾	FCS method coupled with PS P dots	0.025 to 8.0 U/mL	0.025 to 3.0 U/mL	0.025 U/mL
Fluorescence ⁽³³⁾	Silver nanoclusters (Ag NCs) provide FRET	0.1 to 20 U/mL	0.1 to 20 U/mL	0.05 U/mL
Fluorescence ⁽³⁴⁾	FRET probe based on UCNPs and AuNRs	0.08 to 34 U/mL	0.08 to 24 U/mL	0.057 U/mL
Fluorescence ⁽³⁵⁾	Cleavage primer- triggered HRCA	0–70 U/mL U/mL	2.5–70 U/mL	1.8 U/mL
Fluorescence ⁽³⁶⁾	Aggregation- induced emission and template-free DNA polymerization	0-400 U/mL	0.5–100 U/mL	0.16 U/mL
Fluorescence ⁽³⁷⁾	Linear amplification- enhanced exponential amplification strategy	0-8 U/mL	0.125-8 U/mL	0.034 U/mL
ECL ⁽³⁸⁾	CRISPR/Cas12a	5-70 U/mL	0-70 U/mL	23.4 mU/mL
Fluorescence ⁽³⁹⁾	SDA–CRISPR/ Cas12a	0.1–15 U/mL	0.25-1.25 U/mL	$2.458 \times 10^{-3} \text{ U/mL}$
This article	bDTN binds CRISPR/ Cas12a	0-50 U/mL	0.01–1 U/mL	0.001 U/mL

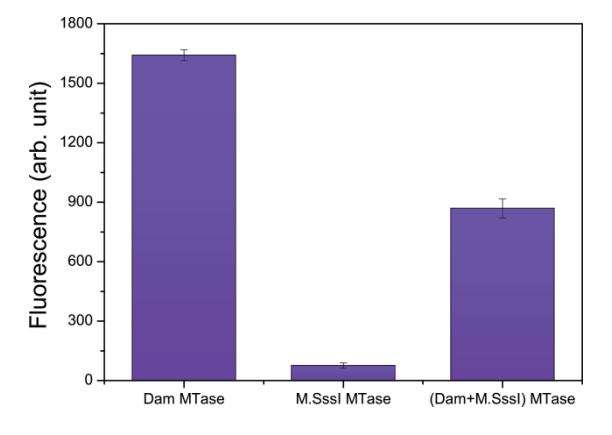


Fig. 5. (Color online) Specificity validation: analysis of methylation activities between Dam MTase and M.SssI MTase. [Error bars indicate SDs; all experiments were independently performed three times (n = 3), with three technical replicates per experiment.]

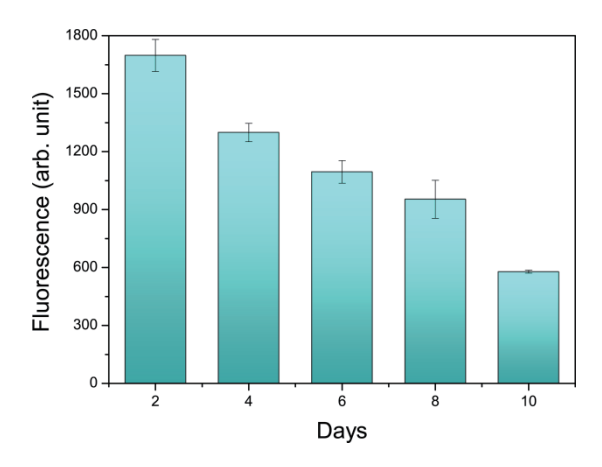


Fig. 6. (Color online) Stability verification from Day 2 to Day 10. [Error bars indicate SDs; all experiments were independently performed three times (n = 3), with three technical replicates per experiment.]

fragments, and perturbations in the system's microenvironment. To enhance the stability of the fluorescent signal, it is advisable to store the system at 4 °C in the dark using a sterile buffer supplemented with antioxidants, which can preserve the effective signal for 5–7 days (maintaining over 50% of the initial intensity). Consequently, experimental materials should be freshly prepared and assayed immediately to ensure the validity of the test results.

3.5 Human serum assay

Dam MTase was introduced into diluted 1% human serum (randomly obtained from Chongqing Jiulongpo District People's Hospital) to perform the DNA methylation reaction, following the same protocol as that of the previous feasibility validation. For the determination of repeatability, three experimental groups were set up with Dam MTase concentrations of 0.01, 0.1, and 1 U/mL. Similarly, 160 μM SAM was added to each group. The recovery ratio (R) was calculated using the formula $R = (C_2/C_1) \times 100\%$, where C_1 represents the theoretically spiked concentration after dilution and C_2 denotes the concentration derived from substituting the assay results into the linear calibration curve. Each concentration was analyzed in three parallel experiments, yielding recoveries of 99, 103, and 110%. The relative SD (RSD%) values were 12, 0.99, and 0.88% (Table 3), indicating good precision of the assay. As a standard evaluation metric, spiked recovery involves introducing a known concentration of the target (e.g., target nucleic acid) into 1% human serum and calculating the ratio of measured concentration to theoretical concentration. Recoveries within the range of 80-120% imply the minimal matrix effect and acceptable anti-interference capability of the method, whereas significant deviations (e.g., <70% or >130%) call for system optimization to mitigate interference. The matrix effect observed in 1% human serum primarily originates from serum components that interfere with Casl2a activity, the stability of fluorescent ssDNA reporter probes, and the reaction microenvironment. The extent of such an effect has been experimentally validated, and its

Table 3
Detection effect of Dam MTase in serum.

Sample no.	$C_1(U/mL)$	$C_2(U/mL)$	Recovery ratio (%) (<i>n</i> =3)	RSD (%)
1	0.01	0.0099	99	12
2	0.1	0.1031	103	0.99
3	1	1.10	110	0.88

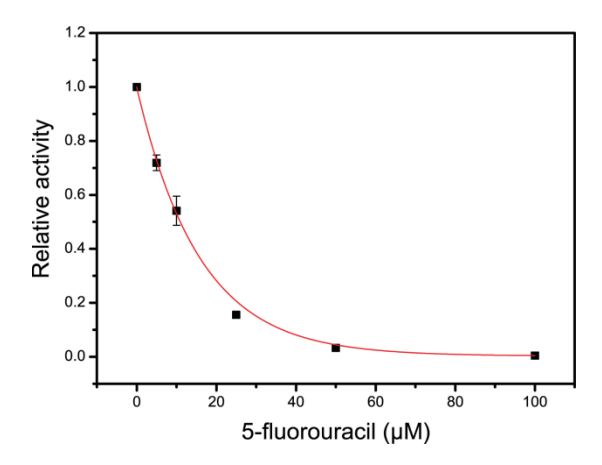


Fig. 7. (Color online) Inhibitory efficacy of 5-FU at various concentrations against 50 U/mL Dam MTase. [Error bars indicate SDs; all experiments were independently performed three times (n = 3), with three technical replicates per experiment.]

impact has been alleviated through system optimization as described in the aforementioned experiments.

3.6 5-FU inhibition assay

For drug screening in disease therapeutics, we validated an enzymatic inhibition assay targeting 5-FU. Aberrant DNA methylation patterns are well-recognized drivers of pathogenesis across diverse diseases, including malignant tumors and carcinomas. Prior studies have established that the selective inhibition of Dam MTase via antibiotic-derived inhibitors can effectively modulate aberrant Dam MTase activity and mitigate pathogenic DNA methylation. As illustrated in Fig. 7, we evaluated five gradient concentrations of 5-FU (5, 10, 25, 50, and 100 μ M) to assess its inhibitory efficacy against Dam MTase, utilizing fluorescent signal attenuation as a readout. Relative activity (RA) was quantified using the formula $RA = (F_2 - F_0)/(F_1 - F_0)$, where F_0 , F_1 , and F_2 represent distinct fluorescence intensities: F_0 corresponds to the signal in the absence of both Dam MTase and 5-FU; F_1 denotes the signal in the presence of 50 U/mL Dam MTase without 5-FU; and F_2 reflects the signal in the presence of 50 U/mL Dam MTase with various concentrations of 5-FU. Both F_1 and the blank value F_0 were derived from the mean of three parallel experiments to ensure robustness in subsequent calculations. At a 5-FU concentration of 100 μ M, the fluorescent signal plateaued at a level approximating the blank control, indicating maximal enzymatic inhibition at this concentration. The half-maximal

inhibitory concentration (IC₅₀) of 5-FU, defined as the concentration required to inhibit 50% of Dam MTase activity, was calculated to be 10.9 μ M. These findings confirm the potent inhibitory effect of 5-FU, highlighting the utility of the proposed strategy for screening candidate MTase inhibitors and its potential as a tool in clinical therapeutics and diagnostics.

4. Conclusions

We have designed a sensitive assay for DNA MTase activity in combination with the CRISPR-Cas system. In this protocol, we first designed the bDTN. The toehold of the DTN is a dumbbell portion with identical structures, and among the four long strands of the bDTN (S1-S4), the 5' ends of S1-S4 are modified with phosphate and the 3' end is hydroxyl. When the T4 DNA ligase acts to form a closed loop during the DNA methylation reaction, in combination with the CRISPR/Cas system, the enzyme cutting reaction produces fluorescence, and the fluorescence intensity is positively correlated with the Dam MTase concentration. Therefore, after optimizing the experimental conditions, we successfully detected Dam MTase at various concentrations (including 0, 0.001, 0.002, 0.004, 0.006, 0.008, 0.01, 0.02, 0.06, 0.1, 0.5, 1, 10, and 50 U/mL). A good linear relationship was observed in the concentration range of 0.01-1 U/mL, with a correlation coefficient (R^2) of 0.99715. Additionally, the LOD was as low as 0.001 U/mL. Compared with recent fluorescence-based detection methods, our approach offers ultrahigh sensitivity, high specificity, and rapid detection. Furthermore, it exhibits a lower false-positive rate and a higher stability than electrochemical and colorimetric methods. Notably, this method has enabled the detection of Dam MTase in human serum and the enzyme inhibitor 5-FU, providing valuable reference for clinical diagnosis and treatment. It also holds clinical significance for the early diagnosis of cancer and other related diseases. Moreover, the successful implementation of this protocol and the validation of Dam MTase as a candidate target offer an important research direction for the broader scientific community.

Acknowledgments

This work was supported by Chongqing Natural Science Foundation (Grant No. CSTB2022NSCQ-MSX0892); the Jiulongpo district-level technology foresight and system innovation project (Grant No. 2023-03-006-Z); the 2024 Chongqing young and middle-aged high-level medical talent project of C.-L. H; the Chongqing medical scientific research project (joint project of Chongqing Health Commission and Science and Technology Bureau) (2024MSXM008 to C.-L. H.); and the postdoctoral research project of Chongqing Natural Science Foundation (CSTB2023NSCQ-BHX0235 to C.-L. H.).

Conflict of interest

The authors declare that they have no known competing financial interests or personal relationships that could have appeared to influence the work reported in this paper.

Authors' contributions

YH: Conceptualization; SD: Methodology; ZC: Validation; HH and ZX: Formal analysis; XY: Data curation; DW: Writing-Original draft; CH and MZ: Writing-Review & editing; MZ: Funding acquisition.

Ethics approval and consent to participate: Not applicable.

Consent for publication: Not applicable.

Competing interests

The authors declare that they have no known competing financial interests or personal relationships that could have appeared to influence the work reported in this paper.

Data availability statement

All data supporting the findings of this study are included within this article and its supplementary information files.

References

- 1 Q. Wen, D. Li, H. Xi, G. Huang, and W. Zhu: J. Pharm. Biomed. Anal. 219 (2022) 114935. https://doi.org/10.1016/j.jpba.2022.114935
- Y. Han, C. Wang, X. Zou, Y. Zhang, Q. Xu, and C. Y. Zhang: Anal. Chem. 94 (2022) 5980. https://doi.org/10.1021/acs.analchem.2c00439
- 3 Y. Kong, L. Cao, G. Deikus, Y. Fan, E. A. Mead, W. Lai, Y. Zhang, R. Yong, R. Sebra, H. Wang, X. S. Zhang, and G. Fang: Science 375 (2022) 515. https://doi.org/10.1126/science.abe7489
- 4 S. Zhang, W. Shi, K. B. Li, D. M. Han, and J. J. Xu: Anal. Chem. **94** (2022) 4407. https://doi.org/10.1021/acs.analchem.1c05332
- 5 W. Zhang, X. Zu, Y. Song, Z. Zhu, and C. J. Yang: Analyst 141 (2016) 579. https://doi.org/10.1039/c5an01763g
- 6 X. Chen, G. Cao, X. Wang, Z. Ji, F. Xu, D. Huo, X. Luo, and C. Hou: Biosens. Bioelectron. 163 (2020) 112271. https://doi.org/10.1016/j.bios.2020.112271
- 7 N. K. MacLennan, S. J. James, S. Melnyk, A. Piroozi, S. Jernigan, J. L. Hsu, S. M. Janke, T. D. Pham, and R. H. Lane: Physiol. Genomics 18 (2004) 43. https://doi.org/10.1152/physiolgenomics.00042.2004
- 8 C. Wenzel and W. Guschlbauer: Nucleic Acids Res. 21 (1993) 4604. https://doi.org/10.1093/nar/21.19.4604
- 9 T. Kimura, T. Asai, M. Imai, and M. Takanami: Mol. Gener. Genet. **219** (1989) 69. https://doi.org/10.1007/BF00261159
- 10 M. N. Giacomodonato, M. N. Llana, M. R. Castañeda, F. Buzzola, M. D. García, M. G. Calderón, S. H. Sarnacki, and M. C. Cerquetti: Microbes Infect. 16 (2014) 615. https://doi.org/10.1016/j.micinf.2014.03.009
- 11 T. Tian, T. Zhang, S. Shi, Y. Gao, X. Cai, and Y. Lin: Nat. Protoc. 18 (2023) 1028. https://doi.org/10.1038/s41596-022-00791-7
- 12 D. Li, Z. Yang, Y. Luo, X. Zhao, M. Tian, and P. Kang: Adv. Healthcare Mater. 11 (2022) e2101412. https://doi.org/10.1002/adhm.202101412.
- 13 K. R. Kim, H. Jegal, J. Kim, and D. R. Ahn: Biomater. Sci. 8 (2020) 586. https://doi.org/10.1039/c9bm01769k.
- 14 Y. Shi, X. Fu, Y. Yin, F. Peng, X. Yin, G. Ke, and X. Zhang: Chem. Asian. J. 16 (2021) 857. https://doi.org/10.1002/asia.202100043.
- 15 Y. Wang, T. Yang, G. Liu, L. Xie, J. Guo, and W. Xiong: Clin. Chim. Acta. 548 (2023) 117520. https://doi.org/10.1016/j.cca.2023.117520.
- N. Liu, R. Liu, and J. Zhang: Bioelectrochemistry 146 (2022) 108105. https://doi.org/10.1016/j.bioelechem.2022.108105.
- 17 L. Lu, B. Liu, J. Leng, and X. Ma: Mikrochim. Acta. **186** (2019) 229. https://doi.org/10.1007/s00604-019-3309-9.

- 18 Y. Zhang, L. Hao, Z. Zhao, X. Yang, L. Wang, and S. Liu: Analyst 145 (2020) 3064. https://doi.org/10.1039/d0an00008f.
- 19 R. Chen, H. Shi, X. Meng, Y. Su, H. Wang, and Y. He: Anal. Chem. 91 (2019) 3597. https://doi.org/10.1021/acs.analchem.8b05595
- 20 X. Luo, T. Kang, J. Zhu, P. Wu, and C. Cai: ACS Sens. 5 (2020) 3639. https://doi.org/10.1021/acssensors.0c02016.
- 21 W. Yuan, K. Xiao, X. Liu, Y. Lai, F. Luo, W. Xiao, J. Wu, P. Pan, Y. Li, and H. Xiao: Anal. Chim Acta 1273 (2023) 341559. https://doi.org/10.1016/j.aca.2023.341559
- 22 H. A. Kermani, M. Hosseini, A. Miti, M. Dadmehr, G. Zuccheri, S. Hosseinkhani, and M. R. Ganjali: Anal. Bioanal. Chem. **410** (2018) 4943. https://doi.org/10.1007/s00216-018-1143-2
- 23 J. Dong, L. He, F. Yu, S. Yu, L. Liu, Y. Tian, Y. Wang, J. Wang, L. Qu, Y. Wu, and R. Han: Luminescence 34 (2019) 368. https://doi.org/10.1002/bio.3619
- 24 Z. Y. Wang, P. Li, L. Cui, Q. Xu, and C. Y. Zhang: Anal. Chem. 92 (2020) 13573. https://doi.org/10.1021/acs.analchem.0c03303
- 25 Z. Qiao, L. Xue, M. Sun, N. Ma, H. Shi, W. Yang, L. Z. Cheong, X. Huang, and Y. Xiong: J. Agric. Food Chem. 72 (2024) 857. https://doi.org/10.1021/acs.jafc.3c07582
- 26 S. Yang, Z. Zhao, B. Wang, L. Feng, J. Luo, R. Deng, J. Sheng, X. Gao, S. Xie, M. Chen, and K. Chang: ACS Appl. Mater. Interfaces 15 (2023) 23662. https://doi.org/10.1021/acsami.3c02614
- 27 Y. Huang, W. Zhang, S. Zhao, Z. Xie, S. Chen, and G. Yi: Anal. Chim. Acta. 1184 (2021) 339018. https://doi.org/10.1016/j.aca.2021.339018
- 28 Q. Wen, D. Li, G. Huang, H. Xi, H. Pan, L. Zhang, Z. Li, X. Xiao, and W. Zhu: Analyst 147 (2022) 4980. https://doi.org/10.1039/d2an01302a
- 29 Z. Li, T. Pi, K. Yang, Z. Xia, Y. Feng, X. Zheng, R. Deng, and B. Chi: Spectrochim. Acta A: Mol. Biomol. Spectrosc. 260 (2021) 119924. https://doi.org/10.1016/j.saa.2021.119924
- 30 X. Xu, L. Wang, X. Li, W. Cui, and W. Jiang: Talanta 194 (2019) 282. https://doi.org/10.1016/j.talanta.2018.09.113
- 31 T. Zhao, X. Pang, C. Wang, L. Wang, Y. Yang, J. Wang, J. Jia, X. Liu, S. Xu, and X. Luo: Anal. Chem. **96** (2024) 4402. https://doi.org/10.1021/acs.analchem.3c04122
- 32 Y. Huang, L. Deng, D. Su, X. Huang, and J. Ren: Analyst 146 (2021) 3623. https://doi.org/10.1039/d0an02362k
- 33 M. Dadmehr, M. A. Karimi, and B. Korouzhdehi: Spectrochim. Acta A: Mol. Biomol. Spectrosc. 228 (2020) 117731. https://doi.org/10.1016/j.saa.2019.117731
- 34 M. Wu, M. Zhang, Z. Fan, X. Qin, X. Zhu, H. Ji, Y. Qin, Q. Wang, and L. Wu: Mikrochim. Acta 188 (2021) 169. https://doi.org/10.1007/s00604-021-04831-z
- 35 L. Chen, Y. Zhang, Q. Xia, F. Luo, L. Guo, B. Qiu, and Z. Lin: Anal. Chim. Acta 1122 (2020) 1. https://doi.org/10.1016/j.aca.2020.04.061
- 36 S. Niu, C. Bi, and W. Song: Anal. Biochem. **590** (2020) 113532. https://doi.org/10.1016/j.ab.2019.113532
- 37 Y. An, Z. Yu, D. Liu, L. Han, X. Zhang, X. Xin, and C. Li: Anal. Bioanal. Chem. **415** (2023) 2271. https://doi.org/10.1007/s00216-023-04647-1
- 38 C. Lin, Q. Huang, M. Tian, F. Luo, J. Wang, B. Qiu, S. Yang, and Z. Lin: Talanta **251** (2023) 123748. https://doi.org/10.1016/j.talanta.2022.123748
- 39 F. Yu, Q. Zhang, T. Ma, S. Zhang, F. Wang, D. Yue, S. Liu, Y. Liao, L. E. Liu, Y. Wu, and W. Zang: Anal. Chim. Acta 1337 (2025) 343540. https://doi.org/10.1016/j.aca.2024.343540